Spatiotemporal analysis of sheet and cloud cavitation and its damage potential

G Hatzissawidis[1], L Kerres[1], G J Ludwig[1] and P F Pelz[1]

[1] Chair of Fluid Systems, Technische Universität Darmstadt, Otto-Berndt-Str. 2, 64287 Darmstadt, Germany

E-mail: peter.pelz@fst.tu-darmstadt.de

Abstract. The cavitation regime has a substantial influence on the damage potential, thus it has to be considered in any specific investigation. For this purpose, we set up a test rig at the Technische Universität Darmstadt using a Circular Leading Edge hydrofoil (CLE) to analyse the damage potential of sheet and cloud cavitation. Exceeding a critical Reynolds number Re_c, the cavitation regime transitions from harmless sheet cavitation to aggressive cloud cavitation. High-speed recordings of the cavitation regime are correlated with high frequency pressure data from a wall-mounted piezoelectric pressure transducer. Spatial and temporal content of the cavitating flow are captured applying proper orthogonal decomposition (POD) to the high-speed recordings. In order to determine the damage potential of the cavitation regime we apply a copper foil on the hydrofoil surface, on which plastic, crater-shaped deformations due to bubble collapses occur. Images of the surface are recorded before and after each run via two-dimensional Pit-Count microscopy. We correlate spatial modes from the cavitating flow field with the eroded surface rate from pitting tests leading to the result that cloud cavitation associated with increasing cloud size is more aggressive. A power law is identified where pitting rate increases with fourteenth power of the Reynolds number.

Keywords: cavitation, cavitation erosion, Pit-Count microscopy, high-speed visualisation, modal decomposition

1. Introduction

Sheet and cloud cavitation are the predominant cavitation regimes occurring in hydraulic machinery like pumps, turbines, propellers as well as in hydraulic components, e.g. heart valves. Due to its transient behaviour cavitation may lead to vibration, noise, decreasing in efficiency as well as mechanical, severe damage of hydraulic components. Extensive experimental and numerical investigations as well as analytical approaches, are conducted and derived contributing to the physical understanding, controlling and predicting of cavitation and cavitation erosion.

Knapp [1] already examined in the 1960s the interaction of the cavitating flow and the underlying crater-shaped deformations called pits. He firstly described the periodic viscous film flow mechanism also known as re-entrant jet which leads to large-scale cloud detachment, advection by the bulk flow, and collapse. The developed method was the first application of Pit-Count microscopy.

Three major experimental fields of research in cavitation erosion emerged during the second half of the last century, classified from generic experiments towards impellers or propellers in pumps or naval applications, respectively: (i) single bubble dynamics in the vicinity of a rigid wall

[2–9], (ii) ultrasonic cavitation in a sonotrode [10–15], (iii) hydrodynamic cavitation in cavitation tunnels in a) a cavitating jet apparatus [16–18], about b) generic geometries such as nozzles [19–23], rotationally symmetrical bodies [1, 24], c) impeller-like hydrofoils [25–29] or d) impellers [25, 30] and propellers [31, 32]. Two ASTM International standards for cavitation erosion tests and the quantification of underlying damage are established using ultrasonic cavitation [33] or a cavitating jet [34].

We conclude that there is a plethora of cavitation erosion experiments, however, we aim at find a trade-off between a generic, representative experiment and the realistic cavitation condition in pumps or naval impellers. For example, the cavitation conditions occurring in the standard tests do not represent the cavitation about impellers or propellers, whereas cavitation erosion tests on particular impeller geometries are associated with two problems. On the one hand, mass loss in reasonable time due to cavitation needs high velocities, which are not achieved in most test rigs, and on the other hand, it is expensive and time-consuming to conduct experiments for each geometry.

To address this, we use a Circular Leading Edge hydrofoil (CLE), Sec. 2.1, which is inspired by the leading edge of a pump impeller blade and focus on both, the cavitating flow and the underlying damage. In numerous works, the cavitation regime is not specified or emphasised, although it plays a major role in the damage potential. Dular et al. [23] synchronise temporal high-speed measurements and Pit-Count. He found out, that various cavitation structures contribute with various amounts to the pit generation, i.e. 95 % of the pits are associated with cavitation clouds, whereas only 5 % are due to bubble collapses at the cavity closure.

To capture spatial and temporal information from the cavitating flow Proper Orthogonal Decomposition (POD), introduced by Lumley [35], is applied to the high-speed frames. Whereas spatial and temporal structures in the regime of the well-known, periodic large-scale cloud cavitation are obvious, sheet cavitation exhibits irregularly small-scale cloud detachments, where periodicity is hidden to the unaided eye. Damage due to cavitation is quantified by scanning the surface after certain intervals by means of Pit-Count microscopy, Sec. 2.2, where the copper foil is used as a sensor.

2. Experimental facility

Experiments are performed in a cavitation tunnel at Technische Universität Darmstadt using high-speed measurement techniques and a high-frequency transducer. To investigate the cavitation appereance, a CLE hydrofoil made of stainless steel was used. The cavitation erosion tests were made on an adapted hydrofoil, which was covered with a copper foil. After certain time intervals, the surface was scanned by the Pit-Count microscope.

2.1. Test rig

The closed-loop cavitation tunnel at Technische Universität Darmstadt is designed for cavitation erosion tests, where velocities up to 30 m/s and pressures up to 16 bar may be achieved Fig. 1 a). Wetted components like vessel, pipes, etc. except for the pump are made from stainless steel to avoid corrosion. The test section has a rectangular cross-sectional area with a height of 70 mm, a depth of 25 mm and a length of 462 mm. The CLE hydrofoil is mounted in the specimen holder and the incidence angle may be adjusted by rotation in the range of $\alpha = 0°$ to 20°, Fig. 1 b). The CLE hydrofoil has a chord length of 40 mm and fill the complete depth, i.e. the span is 25 mm. Side walls are made of acrylic glass to allow optical accessibility of the cavitation appearance.

High-speed measurements in the top view were performed using a IDT Y7-S3 high-speed camera with a Carl Zeiss Makro-Planar T* 2/50 mm ZF lens, operated at a frame rate of 10 000 FPS at 1280×720 pixel resulting in a resolution of $0.04\,\mathrm{mm\,pixel^{-1}}$. Illumination was provided by two Veritas Constellation 120 LED and the exposure time is set to $3.2 - 4.8\,\mu s$.

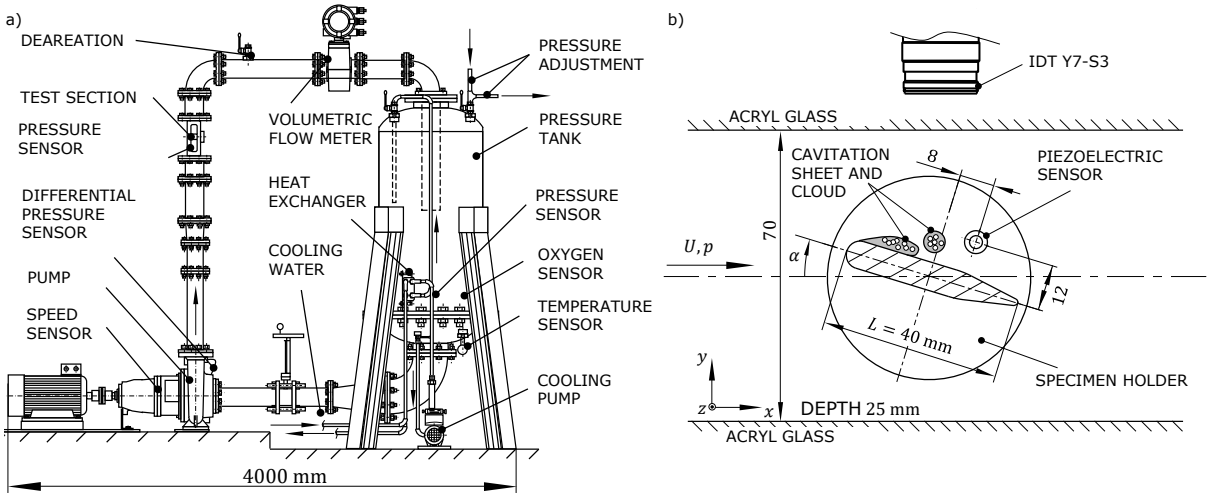

Figure 1. a) Test rig, b) test section with CLE hydrofoil and piezoeletric sensor.

High frequency pressure measurements were conducted in the cloud collapse zone simultaneously with the high-speed recordings using a wall-mounted Kistler Type 601A piezoelectric pressure sensor, eigenfrequency $> 150\,\mathrm{kHz}$, diameter 5.55 mm, c.f. Fig. 1 b), with a Kistler 5015A single-channel charge amplifier at an acquisition rate of 10 kHz for 20 s. Pressure data were recorded using a oscilloscope LeCroy WaveRunner 625Zi, which receives a trigger signal by the high-speed camera.

The operation point is defined by the Reynolds number $Re := U\,L/\nu$ and cavitation number $\sigma := 2\,(p - p_\mathrm{v})/\varrho\,U^2$, where U is the mean bulk flow velocity measured by an ABB ProcessMaster500 FEP511-125D magnetic flow meter, L the chord length of the CLE hydrofoil, ν the kinematic viscosity of water at temperature T, p the static pressure measured by a Keller PAA-33X absolute pressure sensor at an upstream horizontal distance of 143 mm from the hydrofoil midpoint, p_v the vapour pressure and ϱ the density of water at temperature T. The temperature control system keeps the temperature in the range of $T = 23.5\,^\circ\mathrm{C} \pm 0.05\,^\circ\mathrm{C}$. Dissolved oxygen content of the fluid is measured using a VisiFerm DO Arc 120 H0 oxygen sensor mounted in the vessel to ensure equal water quality. The oxygen content within the vessel is kept between 10 and 12 ppm at the begin of all measurements. All data, except for the high frequency pressure data, were recorded using a National Instruments PCIe-6363 card at a sampling rate of 3000 Hz. Measurement uncertainties were estimated according to ISO-GUM using METAS UncLib library in Matlab.

2.2. Pit-Count microscopy

Cavitation damage is determined by Pit-Count microscopy. Microscopic, crater-shaped deformations due to near surface bubble collapses appear in an early stage of cavitation erosion known as incubation phase, in which only plastic deformations are observed, i.e. mass loss is negligible [36]. This method, namely the recording of pits at an early stage, is firstly applied by Knapp [1, 37] and is widely used with measurement techniques capturing two-dimensional [1, 19, 22, 28, 37, 38] or three-dimensional information [20, 24, 39–41], where in the latter the pit depth is included. The advantage of Pit-Count microscopy is that damage potential and the location of the damage can be made without performing time-consuming mass loss measurements.

For this purpose, we develop a two-dimensional Pit-Count microscope, Fig. 2, to scan the pitted CLE hydrofoil surface, automatically. We assume the erosion test time is short enough

such that pits do not overlap and can be clearly delimited from each other, but long enough for a statistical evaluation.

The mean components of the Pit-Count microscope, Fig. 2, are the Basler CMOS sensor with 1280×1024 pixel, scanning an rectangular area of 1.65×1.31 mm and resulting in a resolution of $1.29\,\mu\text{m}\,\text{pixel}^{-1}$, the microscope objective, the collimated LED light source and the electrical cross table with a repeat accuracy of $0.2\,\mu$m. Before each run, the CLE hydrofoil is prepared: a

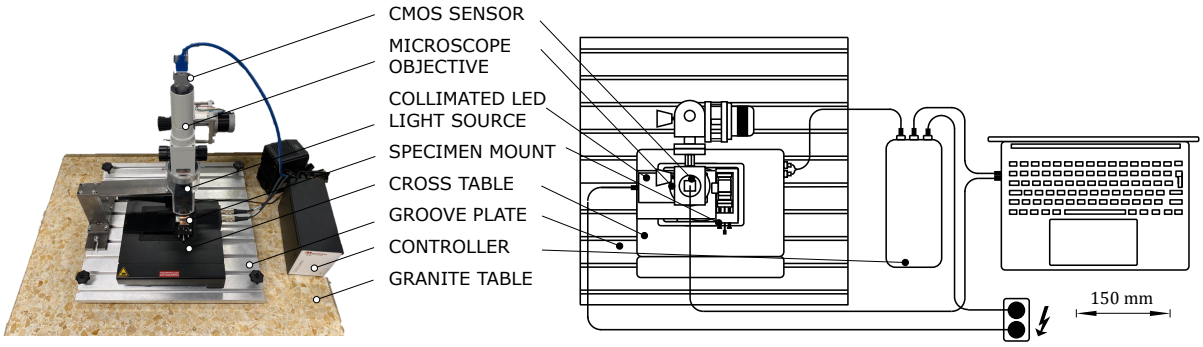

Figure 2. Pit-Count microscope.

milled down CLE hydrofoil made of stainless steel is covered with a copper foil, material name: CU-HCP, tensile strength: 320 MPa, of 200 µm thickness using a adhesive foil of 58 µm thickness and is polished hydraulically smooth, which results in the surface appearing light and the pits dark under the microscope. The mirror finish is necessary and allows the pits to be detected. The plane surface, $22.84\,\text{mm} \times 23.37\,\text{mm}$, of the CLE hydrofoil is scanned in a meandering pattern before and after each run, resulting in 270 single microscope photographs. Good agreement between the results from Pit-Count microscopy and confocal microscopy, model: Sensofar S neox, objective: EPI 20X v35, resolution: $0.69\,\mu\text{m}\,\text{pixel}^{-1}$, is demonstrated in Fig. 3. The region of interest (ROI) of $558\,\mu\text{m} \times 355\,\text{mm}$ denoted in Fig. 3 a) is resolved using confocal microscopy. The identified diameters D_{PC} from Pit-Count microscopy are plotted in the depth profile in Fig. 3 b) demonstrating the good estimation of the two-dimensional Pit-Count method.

3. Results and discussion

3.1. Identification of cavitation regimes

The transition from sheet to cloud cavitation depends on a critical Reynolds number Re_{C}, [42], which is a function of σ and α, $Re_{\text{C}}(\sigma, \alpha)$. Depending on this parameters the cavitation regime can be visually classified into sheet and cloud cavitation, Fig. 4. This leads to stability maps for the incidence angle $\alpha = 2°$ and $6°$, Fig. 5, where cloud cavitation regime is denoted by the grey area. Cloud cavitation exhibits a well-defined periodicity where large-scale clouds are shed from the cavity sheet due to viscous film flow known as re-entrant jet, whereas sheet cavitation regime exhibits irregular shedding of small-scale clouds due to viscous film flow and interfacial instabilities between the sheet and the bulk flow.

We can generally conclude that with increasing Reynolds number and incidence angle cloud cavitation regime is shifted to higher cavitation number, Fig. 5. The stability map describes a *kinematic switch* since this transition depends on the penetration length of the viscous film flow. If the origin of the sheet cavity is reached, cloud cavitation occurs rather than sheet cavitation. In this study we choose for Pit-Count measurements the operation points denoted by the dotted line.

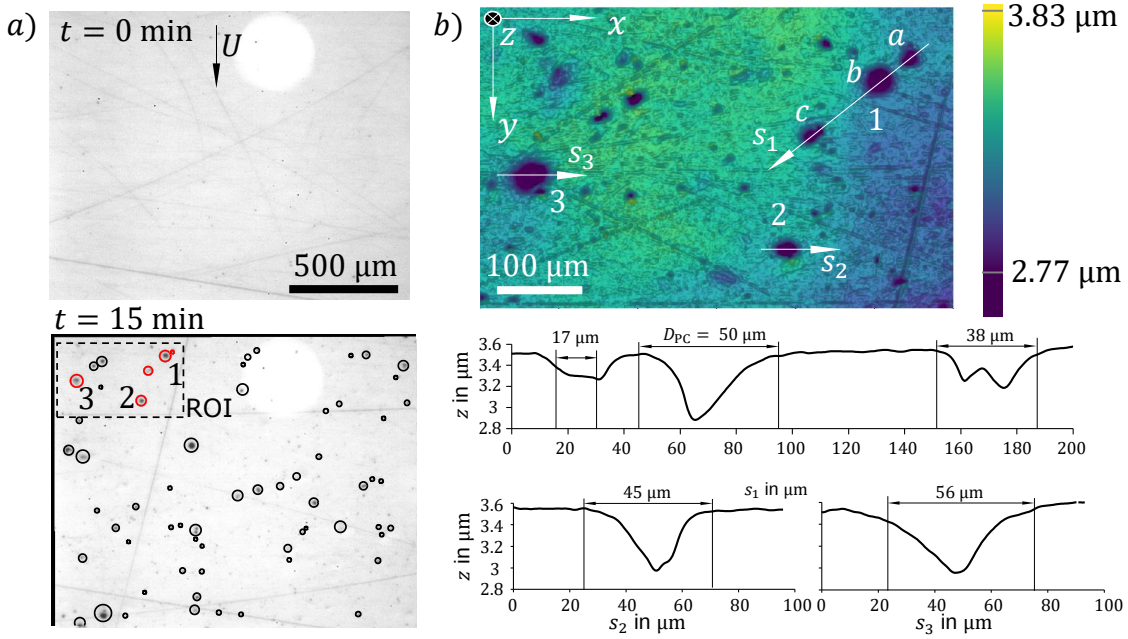

Figure 3. Comparison of a) single microscope photograph from Pit-Count microscopy before and after 15 min of cavitation impact on a copper foil, and b) confocal microscope photography and depth profile of pits within the ROI in a).

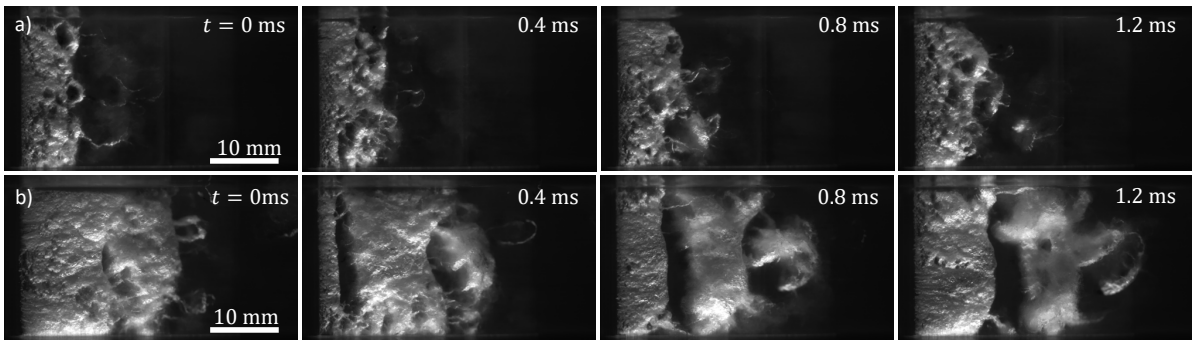

Figure 4. High-speed visualisation about the CLE hydrofoil at $\alpha = 6°$ and $Re = 10 * 10^5$. a) Sheet cavitation at $\sigma = 2$ and b) cloud cavitation at $\sigma = 1.55$.

3.2. Correlation of high-speed recordings, pressure measurements and POD

Fig. 6 shows the normalised pressure $p_+ := (p(t) - \overline{p})/\sigma(p(t))$ and the correlating normalised grey scale intensity $I_+ := -(I(t) - \overline{I})/\sigma(I(t))$ of the high-speed images. $I(t)$ is the recorded signal, where $\overline{(\cdot)}$ and $\sigma(\cdot)$ denotes the mean value and the standard deviation, respectively, cf. [43].

If a cloud passes the piezoelectric sensor the pressure drops due to the circulation of the cloud and as the cloud has a high grey scale the normalised intensity increases (adjusted by the minus sign in the normalised intensity). As it is shown for Fig. 6 a) sheet and b) cloud cavitation, both signals are well matched. The periodicity of cloud cavitation is dominant in the pressure signal. Furthermore, the peaks at $t = 5$ ms and 1.5 ms are due to cloud collapses, immediately after passing the sensor. Since the typical time of the cloud collapse is 0.1 ms, cf. [44], the acquisition

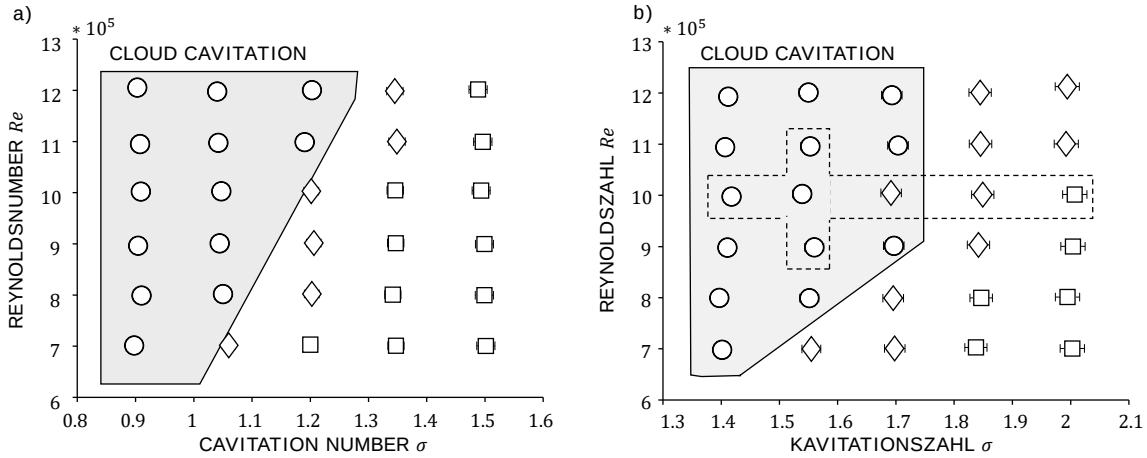

Figure 5. Stability maps for the stainless steel CLE for $\alpha = 2°$ and $6°$, cloud cavitation regime is denoted by circles, transitional regime by diamonds and sheet cavitation regime by squares.

rate of 10 kHz is not sufficient to resolve the cloud collapse phase.

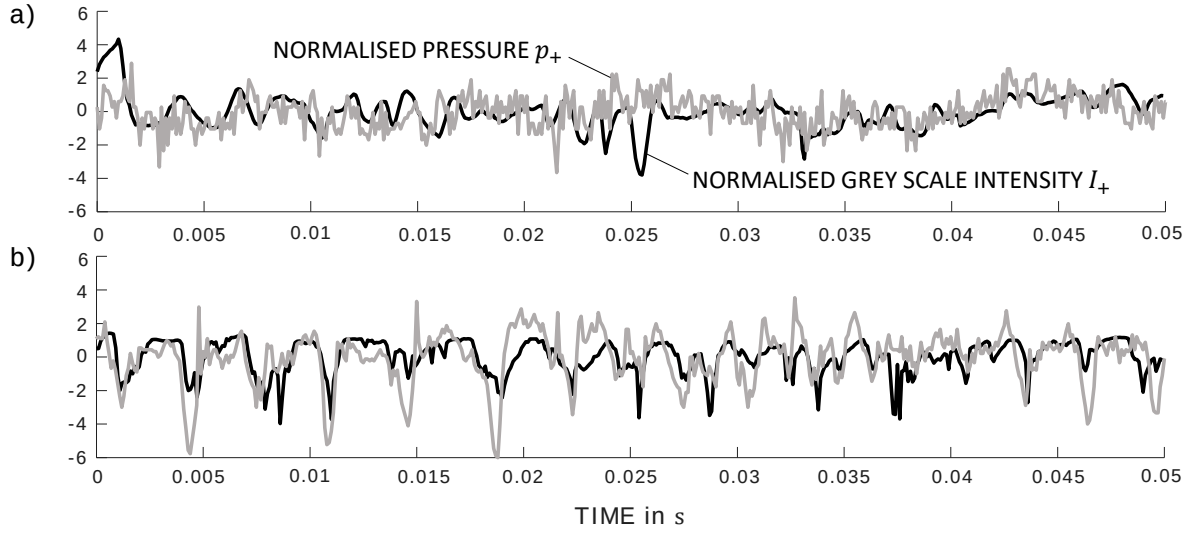

Figure 6. Correlation of the normalised pressure p_+ and grey scale intensity I_+ at $\alpha = 6°$, $Re = 10 * 10^5$. a) Sheet cavitation at $\sigma = 2$ b) cloud cavitation at $\sigma = 1.55$.

Proper Orthogonal Decomposition (POD) more precisely the *method of snapshots*, [45, 46], is applied to 3000 snapshots of high-speed recordings in order to capture spatial modes and corresponding temporal frequencies. The average flow field are subtracted from the single snapshots since we are interested in dynamic phenomena of the cavitating flow field. Usually, input data are velocity fields from PIV measurements, however high-speed recordings as input data are widely used in cavitation research, [47–49]. It should be mentioned that in case of grey scale values as input data, the variance and thus the eigenvalues of covariance matrix do not describe the turbulent kinetic energy, however the corresponding eigenvalue λ_i of mode i may be interpreted as its *information content* – we introduce the relative information content or variance in % as $\lambda_i / \sum_k^N \lambda_k$, where N is the number of snapshots, Fig. 7 a).

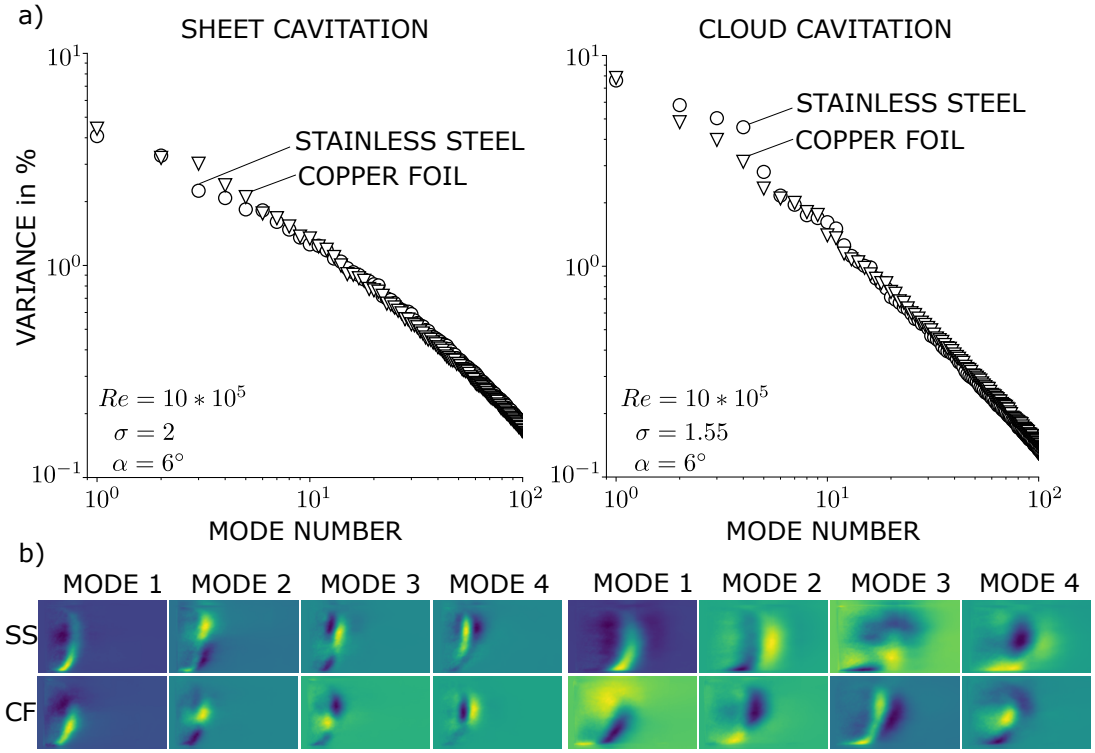

Figure 7. Comparison of the a) variance which can be interpreted as relative information content and b) the corresponding spatial modes of sheet and cloud cavitation regimes between the experiments with the CLE made of stainless steel and the CLE with applied copper foil.

The comparison between the high-speed recordings from the stability maps with the CLE made of stainless steel and pitting tests where the CLE is applied with copper foil does not show a significant influence either in the variance Fig. 7 a) or in the spatial modes Fig. 7 b). It is not surprising that in the case of cloud cavitation, the dominant first modes have a higher variance than in the case of sheet cavitation, since cloud cavitation exhibit a strong periodicity and shedding of large-scale clouds with high information content whereas in the case of sheet cavitation irregular shedding of small-scale clouds is observed. The position of high dynamics is identified from spatial modes, where cavitation erosion is expected, Fig. 7 b) and 8. It should be mentioned that in case of cloud cavitation variances of the 2nd to 5th spatial modes are higher for the CLE applied with copper foil in comparison to the stainless steel CLE, Fig. 7 b) which can be seen in the high-speed recording and in the POD time coefficients (not shown) – cloud shedding is less periodic, i.e. more intermittent, and the corresponding shedding frequency is about 14 % higher in the case of copper foil, 350 Hz and 400 Hz, respectively. This may be related to the modified geometry due to the application of the copper foil, but also to the surface finish where the viscous film flow experiences less dissipation. However, more investigations need to be done to clarify.

3.3. Damage potential

Number and size of pits are captured by means of Pit-Count microscopy and quantify the damage potential of the underlying cavitation regimes discussed in Sec. 3.1 and 3.2. The damage maps, Fig. 8, illustrate the distribution of pits on the plane surface of the CLE hydrofoil for a) sheet and b) cloud cavitation at $Re = 10 * 10^5$. The first order moment of the pit distribution moves

downstream as cavitation number is decrease, whereas due to cloud cavitation and thus strong oscillation of the cavity sheet the second order moment increases, i.e. the damaged area is higher.

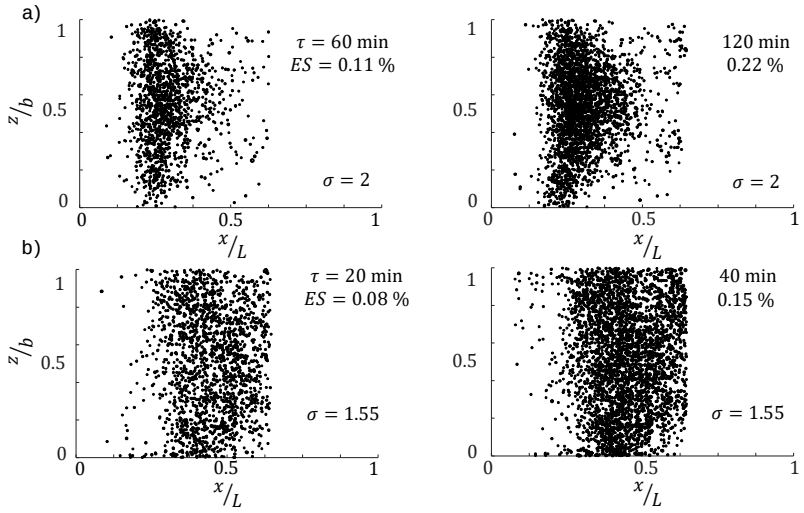

Figure 8. Damage maps at $\alpha = 6°$ and $Re = 10 * 10^5$ for a) sheet cavitation at $\sigma = 2$ after the exposure time of $\tau = 60$, 120 min and b) cloud cavitation $\sigma = 1.55$ after the exposure time $\tau = 20$, 40 min. Pit diameter is amplified by factor 100.

The eroded surface rate ES/τ defined as the pitted surface per surface area and exposure time τ against the cavitation number for constant Reynolds number is shown in Fig. 9 a). Within the transitional regime from the stability maps, Fig. 5, denoted by the grey area, experimental results exhibit at $\sigma = 1.7$ a high variance, whereas in cloud and sheet cavitation regime, experimental results are reproducible and follow a clear progression – cavitation erosion increase as cavitation number decreases. The cavitation regime is sensitive for a small variation in the operation condition within the transitional area leading to undesirable change in cavitation regime for each run, which explain the large spread.

The pitting rate increases with the fourteenth power, $n \approx 14$, of the Reynolds number or velocity, Fig. 9 b). This does not confirm the well-known results of Knapp [1], Stinebring et al. [50] and Belahadji et al. [24], where n is determined to 6 for axissymmetric test bodies. Franc et al. [41] found a relation in power of 5th for a straight nozzle geometry. Following Kim et al. [51], n can vary between 4 and 9. However, the results within this study is much higher. This can be explained by the fact, that we generate aggressive cloud cavitation about a CLE hydrofoil which differs from the geometries used in the literature, thus several cavitation regimes occur influencing damage potential.

4. Conclusion

The influence of cavitation regime on damage potential was investigated by means of high-speed recordings, high-frequency pressure measurements and Pit-Count microscopy. The transition from sheet to cloud cavitation depends on a critical Reynolds number $Re_C = Re_C(\sigma, \alpha)$ and is illustrated in the stability maps, which may be described as a *kinematic switch*. The irregular shedding of small-scale clouds in the sheet cavitation regime and the well-defined periodicity of cloud cavitation is shown through simultaneous high-speed recordings and high-frequency pressure measurements. POD was applied to the high-speed frames. Cloud cavitation shows a higher information content as sheet cavitation in the first modes due to the dominant periodicity

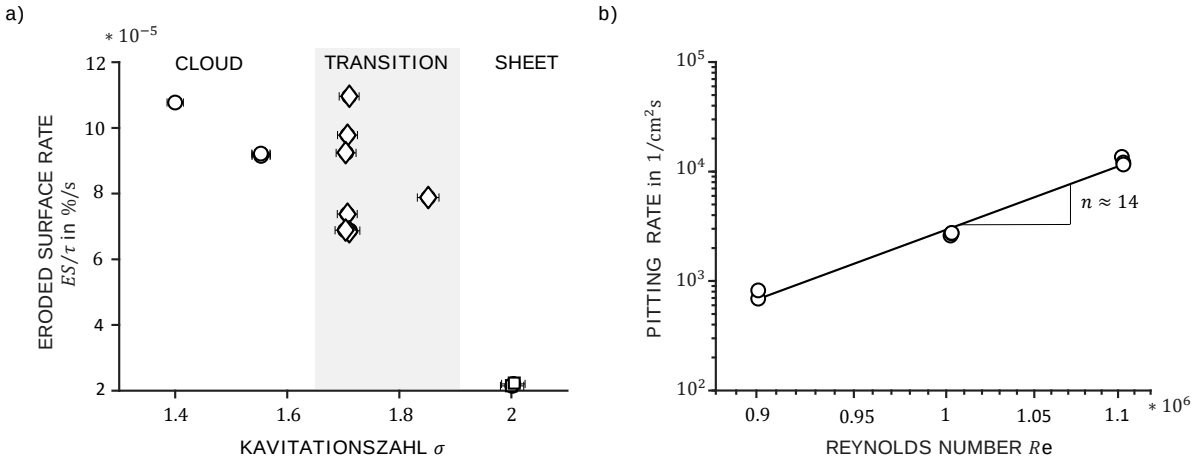

Figure 9. a) Eroded surface rate at $\alpha = 6°$ and $Re = 10 * 10^5$ against σ, b) logarithmic plot of pitting rate against Re at $\alpha = 6°$ and $\sigma = 1.55$.

of large-scale cloud shedding. Regions of high damage potential may be identified from POD spatial modes. A copper foil applied on a CLE was polished hydraulically smooth and used as damage sensor where pits occur. It was figure out that first order moment of damage position occurs at position where high dynamics associated with cloud shedding and collapse is observed. However, the copper foil in comparison with the stainless steel CLE influences the cavitation behaviour due to the variation in surface finish or geometry which is seen within the POD analysis. Cloud cavitation with large-scale cloud shedding exhibits a higher damage potential, however within the transitional cavitation regime eroded surface shows a large spread due to the sensitivity of cavitation behaviour on operation conditions. Furthermore, we found that pitting rate increases with the fourteenth power of the Reynolds number contrary to previous results where n varies from 4 to 9. This can be explained by the fact, that we are using a hydrofoil, whereas in previous investigations axissymmetric test bodies or a straight nozzle were used influencing cavitation damage potential.

5. Acknowledgements

The presented results were obtained within the research project “Numerische Vorhersage des zeitlichen Verlaufes kavitationsbedingter Erosionsschäden zur Erhöhung der Lastflexibilität von Kraftwerkspumpen und Pumpen hoher Leistungsdichte bei gleichzeitig hoher Lebensdauer”, project No. 20395 N/2, funded by the program for promoting the Industrial Collective Research (IGF) of the Federal Ministry for Economic Affairs and Climate Action (BMWK), approved by the Arbeitsgemeinschaft industrieller Forschungsvereinigungen “Otto von Guericke” e.V. (AiF).

Supported by:

Federal Ministry for Economic Affairs and Climate Action

on the basis of a decision by the German Bundestag

References

[1] Knapp R T 1955 *Transaction of the ASME* 1045–1054

[2] Benjamin T B and Ellis A T 1966 *Philosophical Transactions of the Royal Society of London. Series A, Mathematical and Physical Sciences* **260** 221–240 ISSN 00804614 URL http://www.jstor.org/stable/73553

[3] Plesset M S and Chapman R B 1971 *Journal of Fluid Mechanics* **47** 283–290 ISSN 0022-1120

[4] Lauterborn W and Bolle H 1975 *Journal of Fluid Mechanics* **72** 391 ISSN 0022-1120

[5] Blake J R, Taib B B and Doherty G 1986 *Journal of Fluid Mechanics* **170** 479–497 ISSN 0022-1120

[6] Tomita Y and Shima A 1986 *Journal of Fluid Mechanics* **169** 535 ISSN 0022-1120

[7] Kumar S and Brennen C E 1993 *Journal of Fluid Mechanics* **255** 541 ISSN 0022-1120

[8] Philipp A and Lauterbach W 1998 *Journal of Fluid Mechanics* **361** 75–116 ISSN 0022-1120 URL https://www.cambridge.org/core/journals/journal-of-fluid-mechanics/article/cavitation-erosion-by-single-laserproduced-bubbles/F83DCA51380911CD0C4A29CEB65B127D

[9] Lokar Ž, Petkovšek R and Dular M 2021 *Scientific Reports* **11** 3506 ISSN 2045-2322 URL https://www.nature.com/articles/s41598-021-83004-7

[10] Yu-Kang Z and Hammitt F G 1983 *Wear* **86** 299–313 ISSN 00431648 URL https://www.sciencedirect.com/science/article/pii/0043164883901680

[11] Okada T, Iwai Y, Hattori S and Tanimura N 1995 *Wear* **184** 231–239 ISSN 00431648

[12] Hattori S, Mori H and Okada T 1998 *Journal of Fluids Engineering* **120** 179–185 ISSN 0098-2202

[13] Dular M and Osterman A 2008 *Wear* **265** 811–820 ISSN 00431648 URL https://www.sciencedirect.com/science/article/pii/S0043164808000136

[14] Choi J K, Jayaprakash A and Chahine G L 2012 *Wear* **278-279** 53–61 ISSN 00431648

[15] Schreiner F, Hanke S and Skoda R 2021 *Wear* **484-485** 203989 ISSN 00431648 URL https://www.sciencedirect.com/science/article/pii/S004316482100377X

[16] Chahine G L and Courbière P 1987 *Journal of Fluids Engineering* **109** 429–435 ISSN 0098-2202

[17] Soyama H, Futakawa M and Homma K 2005 *Journal of Nuclear Materials* **343** 116–122 ISSN 0022-3115 URL https://www.sciencedirect.com/science/article/pii/S0022311505001194

[18] Hattori S, Hirose T and Sugiyama K 2010 *Wear* **269** 507–514 ISSN 00431648 URL https://www.sciencedirect.com/science/article/pii/S0043164810002322

[19] Hammitt F G 1963 *Journal of Basic Engineering* **85** 347–356 ISSN 0021-9223

[20] Franc J P 2009 *Journal of Fluids Engineering* **131** ISSN 0098-2202 URL https://asmedigitalcollection.asme.org/fluidsengineering/article/131/2/021303/466754/Incubation-Time-and-Cavitation-Erosion-Rate-of

[21] Franc J P, Riondet M, Karimi A and Chahine G L 2011 *Journal of Fluids Engineering* **133** ISSN 0098-2202 URL https://asmedigitalcollection.asme.org/fluidsengineering/article/133/12/121301/455408/Impact-Load-Measurements-in-an-Erosive-Cavitating

[22] Pelz P F, Keil T and Ludwig G 2014 On the kinematics of sheet and cloud cavitation and related erosion *Advanced Experimental and Numerical Techniques for Cavitation Erosion Prediction* (*Fluid Mechanics and Its Applications* vol 106) ed Kim K H, Chahine G, Franc J P and Karimi A (Dordrecht: Springer Netherlands) pp 221–237 ISBN 978-94-017-8538-9

[23] Dular M and Petkovšek M 2015 *Experimental Thermal and Fluid Science* **68** 359–370 ISSN 0894-1777

[24] Belahadji B, Franc J P and Michel J M 1991 *Journal of Fluids Engineering* **113** 700–706 ISSN 0098-2202

[25] Karimi A and Avellan F 1986 *Wear* **113** 305–322 ISSN 00431648 URL https://www.sciencedirect.com/science/article/pii/0043164886900311

[26] Kato H, Konno A, Maeda M and Yamaguchi H 1996 *Journal of Fluids Engineering* **118** 582–588 ISSN 0098-2202

[27] Pereira F, Avellan F and Dupont P 1998 *Journal of Fluids Engineering* **120** 719–727 ISSN 0098-2202

[28] Dular M, Stoffel B and Širok B 2006 *Development of a cavitation erosion model* vol 261 URL https://reader.elsevier.com/reader/sd/pii/S0043164806000494?token=3022341D825832B9A8FE6FAAED735EF440C50FA77B5BC9A6F629093A2B5F1E4C4BE8E67DAE31BD35F9C2673007C84CC5&originRegion=eu-west-1&originCreation=20210922113252

[29] Dular M and Coutier-Delgosha O 2009 *International Journal for Numerical Methods in Fluids* **61** 1388–1410 ISSN 02712091

[30] Joshi S G, Pujari A S, Kale R D and Sreedhar B K 2009 Cavitation studies on a model of primary sodium pump (American Society of Mechanical Engineers Digital Collection) pp 1311–1323 URL https://asmedigitalcollection.asme.org/FEDSM/proceedings/FEDSM2002/36169/1311/296639

[31] Melissaris T, Schenke S, Bulten N and van Terwisga T J 2020 *Wear* **456-457** 203393 ISSN 00431648 URL https://www.sciencedirect.com/science/article/pii/S0043164819316679

[32] Aktas B, Usta O and Atlar M 2020 *Applied Ocean Research* **94** 101868 ISSN 0141-1187 URL https://www.sciencedirect.com/science/article/pii/S0141118718307144

[33] G02 Committee 2017 Astm standard g134-17: Test method for erosion of solid materials by cavitating liquid jet

[34] G02 Committee 2021 Astm standard g32-16(2021)e1: Test method for cavitation erosion using vibratory apparatus

[35] Lumley J L 1970 *Stochastic Tools in Turbulence* (*Applied mathematics and mechanics* vol v. 12) (Burlington: Elsevier Science) ISBN 9780323162258 URL http://gbv.eblib.com/patron/FullRecord.aspx?p=1178477

[36] Franc J P, Chahine G L and Karimi A 2014 Pitting and incubation period *Advanced Experimental and Numerical Techniques for Cavitation Erosion Prediction* (Springer, Dordrecht) pp 37–69 URL https://link.springer.com/chapter/10.1007/978-94-017-8539-6_3

[37] Knapp R T 1958 *Journal of Fluids Engineering* **80** 91–96 ISSN 0098-2202 URL https://asmedigitalcollection.asme.org/fluidsengineering/article/80/1/91/1131679/Accelerated-Field-Tests-of-Cavitation-Intensity?searchresult=1

[38] Escaler X, Farhat M, Avellan F and Egusquiza E 2003 *Wear* **254** 441–449 ISSN 00431648 URL https://www.sciencedirect.com/science/article/pii/S0043164803002618

[39] Patella R F, Reboud J L and Archer A 2000 *Wear* **246** 59–67 ISSN 00431648 URL https://www.sciencedirect.com/science/article/pii/S0043164800004464

[40] Berchiche N, Franc J P and Michel J M 2002 *Journal of Fluids Engineering* **124** 601–606 ISSN 0098-2202 URL https://asmedigitalcollection.asme.org/fluidsengineering/article/124/3/601/444332/A-Cavitation-Erosion-Model-for-Ductile-Materials

[41] Franc J P, Riondet M, Karimi A and Chahine G L 2012 *Wear* **274-275** 248–259 ISSN 00431648 URL https://www.sciencedirect.com/science/article/pii/S0043164811005886

[42] Pelz P F, Keil T and Groß T F 2017 *Journal of Fluid Mechanics* **817** 439–454 ISSN 0022-1120

[43] Barbaca L, Pearce B W, Ganesh H, Ceccio S L and Brandner P A 2019 *Journal of Fluid Mechanics* **874** 483–525 ISSN 0022-1120

[44] Reisman G E, Wang Y C and Brennen C E 1998 *Journal of Fluid Mechanics* **355** 255–283 ISSN 0022-1120

[45] Sirovich L 1987 *Quarterly of Applied Mathematics* **45** 561–571 ISSN 0033-569X URL https://www.ams.org/journals/qam/1987-45-03/S0033-569X-1987-0910462-6/

[46] Holmes P, Lumley J L, Berkooz G and Rowley C W 2012 *Turbulence, coherent structures, dynamical systems and symmetry* 2nd ed Cambridge monographs on mechanics (Cambridge: Cambridge Univ. Press) ISBN 978-1-107-00825-0

[47] Prothin S, Billard J Y and Djeridi H 2016 *Experiments in Fluids* **57** ISSN 0723-4864

[48] Hatzissawidis G, Ludwig G J and Pelz P F 2021 *IOP Conference Series: Earth and Environmental Science* **774** 012097 ISSN 1755-1315 URL https://iopscience.iop.org/article/10.1088/1755-1315/774/1/012097

[49] Hatzissawidis G, Depp B, Ludwig G J and Pelz P F 2021 Modal decomposition of cloud cavitation about a naca 0015 hydrofoil *11th International Symposium on Cavitation* (Daejeon, Korea)

[50] Stinebring D R, Holl J W and Arndt R E A 1980 *Journal of Fluids Engineering* **102** 481–485 ISSN 0098-2202

[51] Kim K H, Chahine G, Franc J P and Karimi A (eds) 2014 *Advanced Experimental and Numerical Techniques for Cavitation Erosion Prediction* Fluid Mechanics and Its Applications (Dordrecht: Springer Netherlands) ISBN 978-94-017-8538-9